

Turbulent Linewidths as a Diagnostic of Self-Gravity in Protostellar Discs

Duncan Forgan ^{1*} Philip J. Armitage ^{2,3} and Jacob B. Simon ²

¹Scottish Universities Physics Alliance (SUPA), Institute for Astronomy, University of Edinburgh, Blackford Hill, Edinburgh, EH9 3HJ, Scotland, UK

²JILA, University of Colorado and NIST, 440 UCB, Boulder, CO 80309-0440, USA

³Department of Astrophysical and Planetary Sciences, University of Colorado, Boulder, USA

Accepted

ABSTRACT

We use smoothed particle hydrodynamics simulations of massive protostellar discs to investigate the predicted broadening of molecular lines from discs in which self-gravity is the dominant source of angular momentum transport. The simulations include radiative transfer, and span a range of disc-to-star mass ratios between $M_d/M_* = 0.25$ and $M_d/M_* = 1.5$. Subtracting off the mean azimuthal flow velocity, we compute the distribution of the in-plane and perpendicular peculiar velocity due to large scale structure and turbulence induced by self-gravity. For the lower mass discs, we show that the characteristic peculiar velocities scale with the square root of the effective turbulent viscosity parameter, α , as expected from local α -disc theory. The derived velocities are anisotropic, with substantially larger in-plane than perpendicular values. As the disc mass is increased, the validity of the α approximation breaks down, and this is accompanied by anomalously large in-plane broadening. There is also a high variance due to the importance of low- m spiral modes. For low-mass discs, the magnitude of in-plane broadening is, to leading order, equal to the predictions from α disc theory and cannot constrain the source of turbulence. However, combining our results with prior evaluations of turbulent broadening expected in discs where the magnetorotational instability (MRI) is active, we argue that self-gravity may be distinguishable from the MRI in these systems if it is possible to measure the anisotropy of the peculiar velocity field with disc inclination. Furthermore, for large mass discs, the dominant contribution of large-scale modes is a distinguishing characteristic of self-gravitating turbulence versus MRI driven turbulence.

Key words: stars: formation, accretion, accretion discs, methods: numerical, radiative transfer, hydrodynamics

1 INTRODUCTION

Protostellar discs are at the heart of both pre-main sequence evolution and planet formation theory. The accretion of the disc material onto young stellar objects (YSOs) is crucial to explaining their phenomenology. This requires angular momentum to be transported outwards, so that mass may be transported inwards (see e.g. Pringle 1981; Lodato 2007; Armitage 2011). Quantitative models of this transport process are needed to describe the evolution of the disc’s surface density profile, the protostar’s accretion rate, the initial conditions for planet formation (Chiang & Youdin 2010), and the subsequent evolution of the planets in the disc. In the simplest description, angular momentum transport is assumed to result from turbulence within the disc, leading to an effective turbulent viscosity (Shakura & Sunyaev 1973),

$$\nu_{\text{eff}} = \alpha c_s H. \quad (1)$$

Here, c_s is the sound speed, H is the scale height, and α is a parameter that characterizes the efficiency of the transport. Constraints from observed disc lifetimes and accretion rates (Hartmann et al. 1998) are consistent with models in which $\alpha \sim 10^{-2}$.

Protostellar disc angular momentum transport is thought to result from two different mechanisms (depending on the location and time in the disc’s evolution). In regions of sufficiently high levels of ionization, the magnetorotational instability (MRI) is a plausible source of turbulence (Balbus & Hawley 1991, 1998; Papaloizou & Nelson 2003). Further out in the disc (or early on when the disc is quite massive), the disc may be cool and massive enough that the disc’s own self-gravity is the dominant source of turbulence (Lin & Pringle 1987; Laughlin & Bodenheimer 1994). This requires that the Toomre Q parameter (Toomre 1964; Durisen et al. 2007),

$$Q = \frac{c_s \kappa}{\pi G \Sigma} < 1.5 - 1.7 \quad (2)$$

where κ is the epicyclic frequency ($\kappa = \Omega$ for Keplerian discs), and Σ is the disc surface density. Discs with large Q will undergo radia-

* E-mail: dhf@roe.ac.uk

tive cooling towards lower values. The onset of non-axisymmetric instability produces spiral structures in the disc, heating it through shocks and viscous-scale dissipation. Typically, self-gravitating discs will reach a self-regulated, quasi-steady state referred to as marginal instability (Paczynski 1978), where the heating and cooling are in approximate balance, and $Q \sim 2$. This produces a self-sustaining *gravito-turbulence*, which can be described by an effective α (Gammie 2001; Lodato & Rice 2004), although there are circumstances where this approximation fails (Forgan et al. 2011). It is also possible that both MRI and self-gravitating turbulence could be generated at the same time, particularly in the case of layered accretion discs (Gammie 1996; Armitage et al. 2001; Zhu et al. 2009; Martin & Lubow 2011).

Determining *observationally* which mechanism is driving transport at a particular radius in a disc is difficult. Although the condition for the onset of self-gravity (Equation 2) is simple and well-understood, measuring Q requires an absolute determination of the gas surface density as a function of radius. This is hard. Most disc mass estimates are derived from dust tracers, which may be systematically biased (Andrews & Williams 2007). Independent observational discriminants of turbulence would therefore be very valuable.

One promising route is to detect the turbulent broadening of molecular lines in the infrared and/or sub-mm. For local fluid turbulence, elementary arguments (Balbus & Hawley 1998) suggest that the characteristic velocity perturbations will be of order $v \sim \sqrt{\alpha} c_s \sim 0.1 c_s$. Using shearing box simulations of MHD turbulence, Simon et al. (2011) show that this is indeed the approximate value of velocity perturbations at the disc midplane, but that a few scale heights above the midplane they can be as high as $0.5 c_s$, and that a small fraction of the broadening is in fact supersonic. While extracting turbulent broadening for molecular species directly from the simulations would be ideal, doing so requires an understanding of the disc's density and temperature fields and the abundance of the molecular lines in question. Modelling these properties in observations is non-trivial, as is the subsequent modelling of radiation transport through the disc. Projection and resolution effects must also be considered. Having said this, recent observations have successfully constrained turbulent broadening. For example, using the CO (3-2) transition with the Sub Millimetre Array (SMA), Hughes et al. (2011) placed an upper limit of $v < 0.1 c_s$ in the TW Hydra system and determined a broadening value of $v \approx 0.4 c_s$ in HD 163296. With the advent of more sensitive millimetre instruments such as ALMA, these constraints will be significantly improved upon.

In this paper, we present preliminary calculations of turbulent velocities in global, three-dimensional smoothed particle hydrodynamics simulations of self-gravitating protostellar discs with radiative transfer (Forgan et al. 2009). Our goal is to characterise the turbulent velocity distribution to first-order, and identify any qualitative features in the turbulent velocity field that might enable the discrimination between alternate mechanisms for driving turbulence (although we leave the extraction of synthetic line observations for future work). Existing studies of the MRI and of self-gravitating turbulence suggest that significant differences may exist. Although large-scale magnetic fields play a role in MHD turbulence (Simon et al. 2012), the MRI can be described to a first approximation as a local angular momentum transport mechanism. The same is not true of self-gravity in the limit where the disc is massive (Balbus & Papaloizou 1999; Lodato & Rice 2005; Forgan et al. 2011). With this in mind, we seek to identify phenomenological differences which would allow us to distinguish

whether line-broadening is MHD-driven or gravity-driven. Such a discriminant would be complementary to estimates based upon derived disc masses, or upon direct imaging searches for spiral structure (Cossins et al. 2010).

2 METHOD

2.1 SPH and the Hybrid Radiative Transfer Approximation

Smoothed Particle Hydrodynamics (SPH) (Lucy 1977; Gingold & Monaghan 1977; Monaghan 1992) is a Lagrangian formalism that represents a fluid by a distribution of particles. Each particle is assigned a mass, position, internal energy and velocity. State variables such as density and pressure are then calculated by interpolation (see reviews by Monaghan 1992, 2005). In the simulations presented here, the gas is modelled using 500,000 SPH particles while the star is represented by a point mass particle onto which gas particles can accrete, if they are sufficiently close and are bound (Bate et al. 1995).

The SPH code used in this work is based on the SPH code developed by Bate et al. (1995) which uses individual particle timesteps, and individually variable smoothing lengths, h_i , such that the number of nearest neighbours for each particle is 50 ± 20 . The code uses a hybrid method of approximate radiative transfer (Forgan et al. 2009), which is built on two pre-existing radiative algorithms: the polytropic cooling approximation devised by Stamatellos et al. (2007), and flux-limited diffusion (e.g., Whitehouse & Bate 2004; Mayer et al. 2007, see Forgan et al. 2009 for details). This union allows the effects of both global cooling and radiative transport to be modelled, without imposing extra boundary conditions.

The opacity and temperature of the gas is calculated using a non-trivial equation of state. This accounts for the effects of H_2 dissociation, H^0 ionisation, He^0 and He^+ ionisation, ice evaporation, dust sublimation, molecular absorption, bound-free and free-free transitions and electron scattering (Bell & Lin 1994; Boley et al. 2007; Stamatellos et al. 2007). Heating of the disc is achieved by $P dV$ work and shock heating. Stellar irradiation is not included as a heating source.

2.2 Initial Disc Conditions

The gas discs used in this work were initialised with the 500,000 SPH particles located between $r_{\text{in}} = 10$ au and $r_{\text{out}} = 50$ au, distributed such that the initial surface density profile is $\Sigma \propto r^{-3/2}$ and the initial sound speed profile is $c_s \propto r^{-1/4}$. They were first presented in Forgan et al. (2011) to evaluate the validity of the α -approximation.

We are primarily interested in considering quasi-steady self-gravitating systems, rather than systems that could fragment to form bound companions. These initial conditions (in particular the small disc radii) were therefore motivated by recent work suggesting that massive discs will fragment at radii beyond $\sim 60 - 70$ au (Rafikov 2005; Stamatellos et al. 2007; Stamatellos & Whitworth 2008; Clarke 2009; Rice & Armitage 2009). This result is consistent with observations that massive discs tend to have outer radii less than 100 au (Rodríguez et al. 2005). A summary of the disc parameters investigated can be found in Table 1. Simulation 1, as the lowest mass disc in the set, approximates local angular momentum transport; Simulation 4 exhibits strongly non-local angular momentum transport. The strength of non-local effects increases as the

Table 1. Summary of the disc parameters investigated in this work.

Simulation	M_* (M_\odot)	M_d (M_\odot)
1	1.0	0.25
2	1.0	0.5
3	1.0	1.0
4	1.0	1.5

disc mass is increased, indicated by increasing amplitude in $m = 2$ spiral modes (see Figure 1).

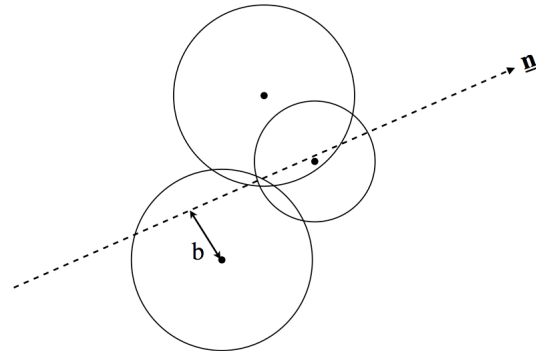
2.3 Calculating line of sight velocities

Observational constraints on turbulence (or, more generally, on deviations from Keplerian rotation) are derived from two-dimensional maps of the line of sight velocity field as traced by a particular molecular line. Two distinct theoretical quantities that can be derived from our simulations are relevant for comparing against such measurements. One possibility is to compute the density (or volume) weighted distribution of line of sight velocity along columns that penetrate the disc. This metric would probe only the small-scale turbulent velocity field. Our SPH simulations are not best-suited to capturing this component accurately, and current observational techniques do not resolve these scales (Hughes et al. 2011). Alternatively, we can subtract off the contribution to the line of sight velocity from the mean azimuthal flow, and evaluate the distribution of the peculiar velocity field that remains. This peculiar velocity field *results from* the presence of turbulence within the disc (since by construction we have removed the velocity of a laminar circular disc), but it need not be the same as the local turbulent broadening. In particular, for a massive self-gravitating disc, significant contributions to the peculiar velocity field arise from low-order azimuthal disc structure, i.e. the spiral arms. We select the second metric as it better reflects the observables currently available.

To compute the distribution of line of sight peculiar velocity, we raytrace through the SPH simulation using the algorithms described in Altay et al. (2008) and Forgan & Rice (2010). Particles only contribute to the density and velocity fields along the ray if their smoothing volumes¹ intersect it (see figure 2).

As the smoothing volume is spherical, the task of determining intersections is reduced to determining the closest approach of a ray to a particle (i.e., the impact parameter b , as labelled in figure 2), and comparing it with the particle’s smoothing length h . If $b < 2h$, then the particle’s smoothing volume is intersected, and its properties are used in the calculation.

Multiple rays are drawn through a region delineated by an annulus on the disc surface, allowing an azimuthally averaged sampling of the velocity field while minimising the effects of particle disorder and Poisson noise. A total of 250,000 rays are drawn for each run, ensuring that almost all particles contained within the annulus are intersected by at least one ray. We obtain the mean velocity in the annulus - in both the vertical direction (v_z), and in the plane of the disc (v_p) - and subtract this to obtain the peculiar velocity field for all particles in the annulus. We then return to the list


Figure 2. Illustrating the raytracing method. Particles only contribute to the estimated line of sight velocity if their smoothing volume intersects the ray. Figure taken from Forgan & Rice (2010).

of particles intersected by the 250,000 rays, and perform a density-weighted average of the peculiar velocities, in the same fashion as Simon et al. (2011). This is a first-order approximation to the emissivity of the gas (i.e., we expect denser regions to radiate more than less dense regions).

By binning the density-weighted peculiar velocity of each particle in the list, we can construct a probability distribution of velocities normalised by the local sound speed, $P(v/c_s)$. These linewidth probability distributions (LPDs) are not equivalent to any observed line profile, but instead give the probability of observing a particular linewidth. Unlike Simon et al. (2011), we do not perform time averages of these LPDs (although how the LPD varies with time can be seen in section 3.3).

2.4 Limitations due to spatial resolution

The global disc simulations that we use in this work necessarily have lower spatial resolution than local, shearing-box simulations. Additionally, the use of constant mass SPH resolution elements naturally concentrates what spatial resolution we do have toward the disc midplane, where the bulk of the mass is. These properties of the simulations result in two limitations that we need to be mindful of. First, we cannot study a radial extent that is too broad, because this would result in regions where the low particle density compromises the resolution of physical angular momentum transport processes. Second, we cannot study the vertical dependence of the turbulent velocity at heights where we have too few resolution elements.

The limitation in the radial extent over which the simulation is trusted worthy derives from the use of artificial viscosity. While required by the SPH code used, the magnitude of artificial viscosity must be quantified so that we know where in the disc the artificial viscosity is likely to be lower than the effective viscosity generated by the gravitational instabilities. The linear term for the artificial viscosity can be expressed as (Artymowicz & Lubow 1994; Murray 1996; Lodato & Price 2010):

$$\nu_{\text{art}} = \frac{1}{10} \alpha_{\text{SPH}} c_s h, \quad (3)$$

where c_s is the local sound speed, h is the local SPH smoothing length, and α_{SPH} is the linear viscosity coefficient used by the SPH code (taken to be 0.1). We can define an effective α param-

¹ The smoothing volume is a sphere of radius $2h_i$, where h_i is the smoothing length of particle i

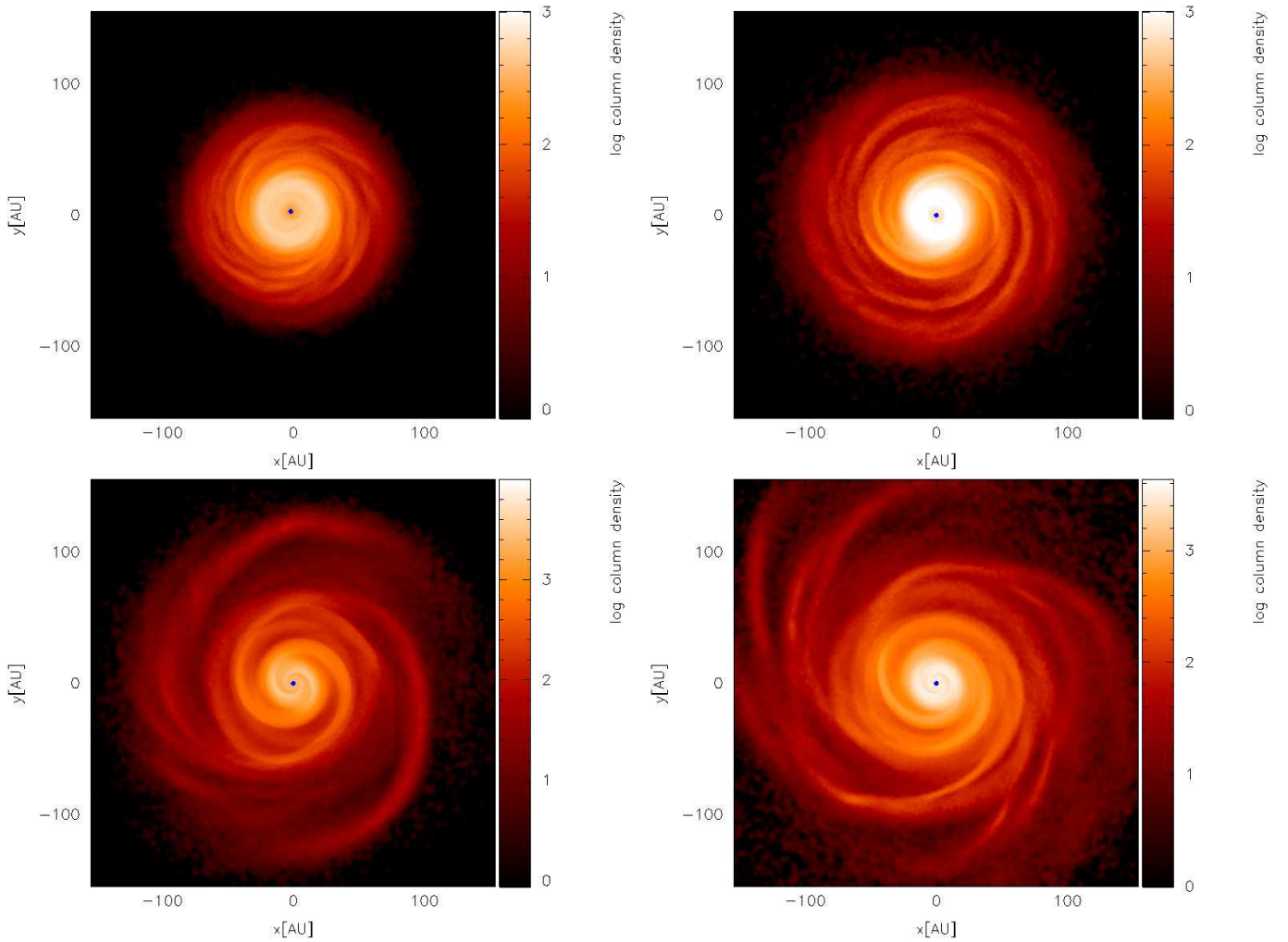


Figure 1. Images showing the surface density structure of Simulations 1 (top left), 2 (top right), 3 (bottom left) & 4 (bottom right) after 27 outer rotation periods (ORPs). The stellar mass in each case is $1 M_{\odot}$, and the initial disc masses of $0.25 M_{\odot}$, $0.5 M_{\odot}$, $1 M_{\odot}$ and $1.5 M_{\odot}$ respectively. The axis ranges are shown in each figure - it is clear that the more massive discs exhibit higher amplitude spiral structures, in particular the $m = 2$ mode.

eter associated with the artificial viscosity by using equation (1) (Lodato & Rice 2004; Forgan et al. 2011)

$$\nu_{\text{art}} = \alpha_{\text{art}} c_s H, \quad (4)$$

and hence combining equations (3) and (4) gives (Artymowicz & Lubow 1994; Murray 1996; Lodato & Price 2010)

$$\alpha_{\text{art}} = \frac{1}{10} \alpha_{\text{SPH}} \frac{h}{H}. \quad (5)$$

This shows that where the vertical structure is not well resolved (i.e., $\frac{h}{H}$ is large), artificial viscosity will dominate. In the simulations presented here, this is typically the case inside ~ 10 au (see Forgan et al. 2011 for details), so any data inside this region can not be used. We therefore did not initially populate the region inside 10 au and although particles will move inside 10 au during the course of the simulations, we only consider results outside this radius.

There are also limitations in the vertical direction. Unlike Simon et al. (2011), the simulations are not well resolved above two scale heights, so we are unable to comment on how turbulent velocities evolve at higher altitudes, and must be satisfied with mid-plane data only. Figure 3 shows an attempt to measure the LPD in

v_p at the midplane, and at one scale height above it. The curves are remarkably similar, but the poor resolution of higher altitudes forbids us from attributing this to any phenomenology of the disc.

3 RESULTS

In this section, we describe the dependence of the discs' peculiar velocity fields on the disc mass, radius, and time from the simulations.

3.1 Dependence on Disc Mass

As previously stated, the underlying disc mass may not be correctly estimated by observations - can turbulent linewidths help break this degeneracy? Figure 4 shows the LPDs for all four simulations (where the annulus was placed at 25 au, with rays projected vertically through the disc).

From Figure 4 in (Forgan et al. 2011), the time averaged α values at 25 au for these four discs range between $\sim 0.005 - 0.01$. Comparing the in-plane (v_p) distributions to these values, we find that Simulation 1 has a mode at $v/c_s \sim \sqrt{\alpha}$, as might be expected

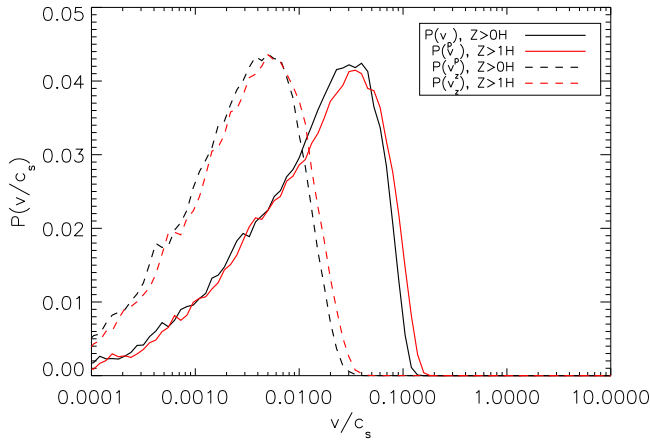


Figure 3. The linewidth probability distribution in v_p for Simulation 1, with $r = 25$ au. Planar velocities v_p are plotted in solid lines, vertical velocities v_z are plotted in dashed lines.

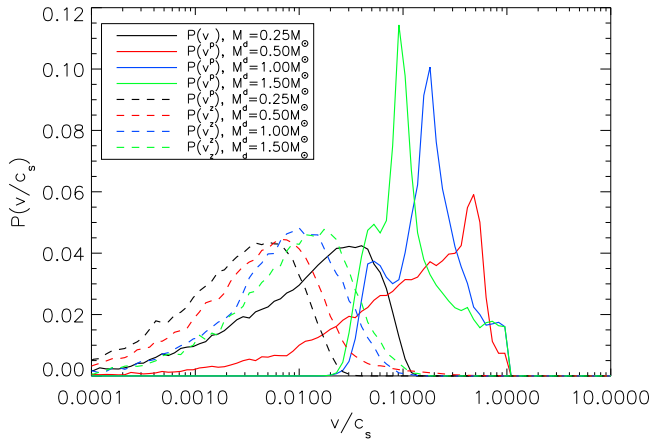


Figure 4. Linewidth probability distributions for all four simulations, where rays are drawn through $r = 25$ au. Planar disc velocities v_p are drawn in solid lines, and vertical velocities v_z are drawn in dashed lines.

from α -disc theory. However, increasing the disc mass appears to break this relation, which is a symptom of the α -approximation itself beginning to break down in the face of non-local angular momentum transport (Balbus & Papaloizou 1999; Forgan et al. 2011). The LPDs change shape dramatically, developing strong peaks and strongly asymmetric profiles. These profiles appear to be tracing the low-order $m = 2$ spiral arms as can be seen in the lower panels of Figure 1. Despite this, there is a strong cutoff at $v/c_s = 1$. This is due to the subtraction of the average planar motion, which for self-gravitating discs at marginal instability is $v/c_s = 1$ (Cossins et al. 2009).

The v_z distributions are much more orderly, with the mode increasing by around one order of magnitude as the disc mass is increased by a factor of 5. The shape of these profiles is also reasonably constant.

3.2 Dependence on Disc Radius

Having seen the striking change in LPD as the disc mass is increased and low- m spiral modes begin to significantly affect line broadening, it is instructive to compare how LPDs change as different disc radii are probed.

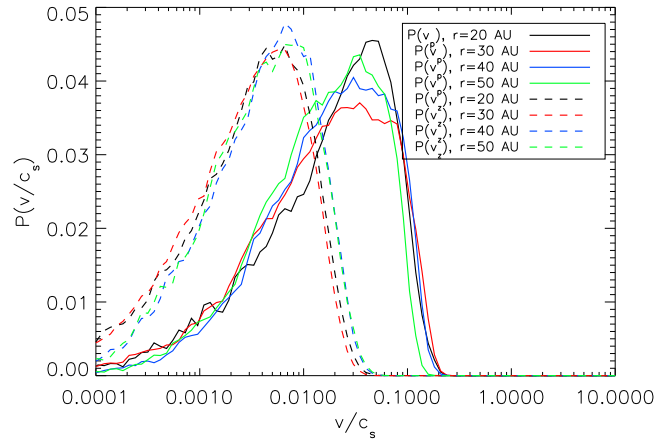


Figure 5. Linewidth probability distributions for Simulation 1, where rays are drawn at a variety of radii. Planar disc velocities v_p are drawn in solid lines, and vertical velocities v_z are drawn in dashed lines.

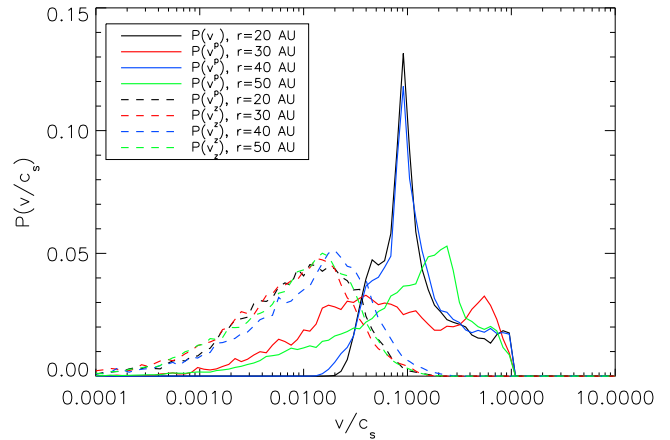


Figure 6. Linewidth probability distributions for Simulation 4, where rays are drawn at a variety of radii at zero inclination. Planar disc velocities v_p are drawn in solid lines, and vertical velocities v_z are drawn in dashed lines.

Figure 5 shows LPDs for Simulation 1, drawn at a variety of disc radii.² In this low mass case, the difference in peak between planar and vertical LPDs remains constant across all radii. Indeed, both LPDs remain very similar across all radii. The α profile of Simulation 1 begins to flatten out towards a constant value beyond $r \sim 30$ au (see Forgan et al. 2011), which would presumably explain why the peaks of the LPDs tend towards similar values (as the characteristic velocity $v/c_s \sim \sqrt{\alpha}$).

The situation is somewhat different for Simulation 4 (Figure 6). As the radius increases, the presence or absence of a spiral arm inside the annulus strongly affects the observed LPD for v_p . Annuli containing an arm have a strong spike, with a much narrower dispersion in v/c_s . Annuli which do not contain arms possess broader LPDs. Notably, the v_z distributions remain unchanged, although this may be symptomatic of low vertical resolution, and as such we should be wary of denoting this as a phenomenological effect.

² Due to numerical limitations, we are restricted to a relatively small range in radii compared to the studies of Simon et al. (2011); see Section 2.4.

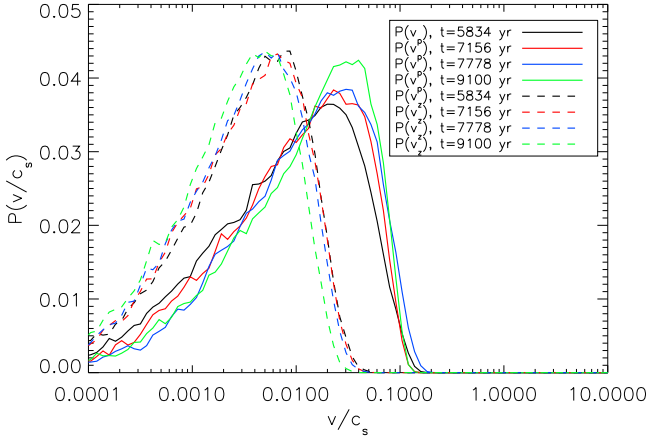


Figure 7. Linewidth probability distributions as a function of time for Simulation 1. Rays are drawn at $r = 25$ au. Planar disc velocities v_p are drawn in solid lines, and vertical velocities v_z are drawn in dashed lines.

3.3 Time Dependence

Finally, it is expected that linewidths should be able to probe the inherent variability in these self-gravitating discs. As is shown in Forgan et al. (2011), Simulation 1 exhibits low variability, and Simulation 4 exhibits high variability. These features can be detected by calculating the LPD at a series of timesteps throughout the disc’s evolution.

The LPDs of Simulation 1 remain stable over several thousand years (Figure 7), with the differences for both v_p and v_z being little more than extremely small shifts in the value of the peak. The systematic separation between v_p and v_z is maintained as a result.

By contrast, the v_p LPD for Simulation 4 (Figure 8) fluctuates much more noticeably, with both the shape of the LPD and the amplitude of the peaks shifting over time. This is again due to the passage of strong $m = 2$ features through this particular radius.

Observers hoping to construct LPDs by observing objects should take note. These results would suggest that such efforts would be successful for low mass discs, but the increased variability would rule this method out for high mass discs. Conversely, the simulations show that variability can be seen in higher mass discs, even at this comparatively low resolution.

Again, we see very little change in the v_z LPD across all disc masses, but we must be cautious as these distributions are the most sensitive to resolution issues.

3.4 Dependence on Numerical Resolution

Finally, we compare the effects of increasing particle number on the resulting LPDs. Simulation 1 was rerun with 1 million particles (double the previous value), and LPDs were investigated at the same instant as a function of radius. Due to computing constraints, the high resolution simulation was not run for the same number of outer rotation periods as the low resolution simulation. In Figure 9 we compare the two resolutions at the same simulation time of approximately 3500 years.

The general features of the LPDs are robust - the position of the peaks remains at similar values. The v_z distributions remain very much the same, despite increasing the vertical resolution by around 25%. Strong differences can be seen in the outer disc radii (blue and green curves). This is due to extra resolution having a stronger effect at lower particle densities. The inner disc regions

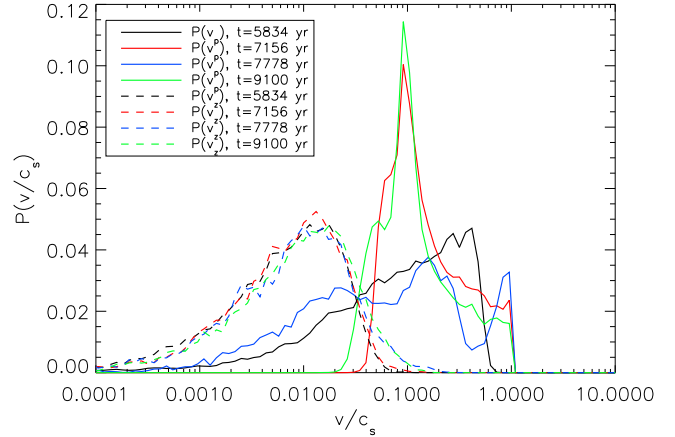


Figure 8. Linewidth probability distributions as a function of time for Simulation 4. Rays are drawn at $r = 25$ au. Planar disc velocities v_p are drawn in solid lines, and vertical velocities v_z are drawn in dashed lines.

still display systematic separation of v_p and v_z , although the amplitude of the peaks in v_p do change by around 10%.

4 DISCUSSION & CONCLUSIONS

We have presented preliminary studies of turbulent line broadening due to self-gravity using global smoothed particle hydrodynamics (SPH) simulations of protostellar discs. With radiative transfer included in these calculations, we carried out raytracing techniques to measure the local velocity components in the disc plane and transverse to the disc plane (relative to the local sound speed). From these raytracing measurements, we construct a linewidth probability distribution (LPD) which gives the probability of detecting lines broadened to a given width. These simulations cannot resolve turbulence at scales below the smoothing length, and artificial viscosity effects will also smooth out turbulence to a lesser extent. That being said, we have detected some promising diagnostics that can be compared to current MRI-driven turbulence simulations but that will require follow-up with high resolution studies.

First, we have found that the LPD is noticeably mass dependent, with the maximum value of v/c_s increasing towards $v/c_s = 1$, where there is a strong cutoff. Non-local angular momentum transport is evident from strong peaks in the distribution in v_p being caused by low- m spiral structure impinging on the disc radii being observed. This behaviour becomes apparent when the same disc is compared at various radii of observation.

Low mass discs which possess weaker, high m spiral structure retain similar LPDs at all radii, with a systematic separation between the peak of the v_z distribution and the peak of the v_p distribution; v_p peaks near $\sim 0.04c_s$, whereas v_z peaks near $\sim 0.005 - 0.01c_s$.

The results from this work can be compared with the work of Simon et al. (2011) as a way to extract potential differences between the LPDs of MRI-driven turbulence and motions due to self-gravity. First, comparing the actual mid-plane values of v/c_s , we find roughly the same (though somewhat lower) peak v_p/c_s in our low mass discs compared to MRI-driven discs in the ideal MHD limit (Simon et al. 2011). However, the peak values of v_p/c_s in this work are slightly larger than the dead-zone values of the 4 au simulation of Simon et al. (2011).

The largest difference between the LPDs of low mass self-

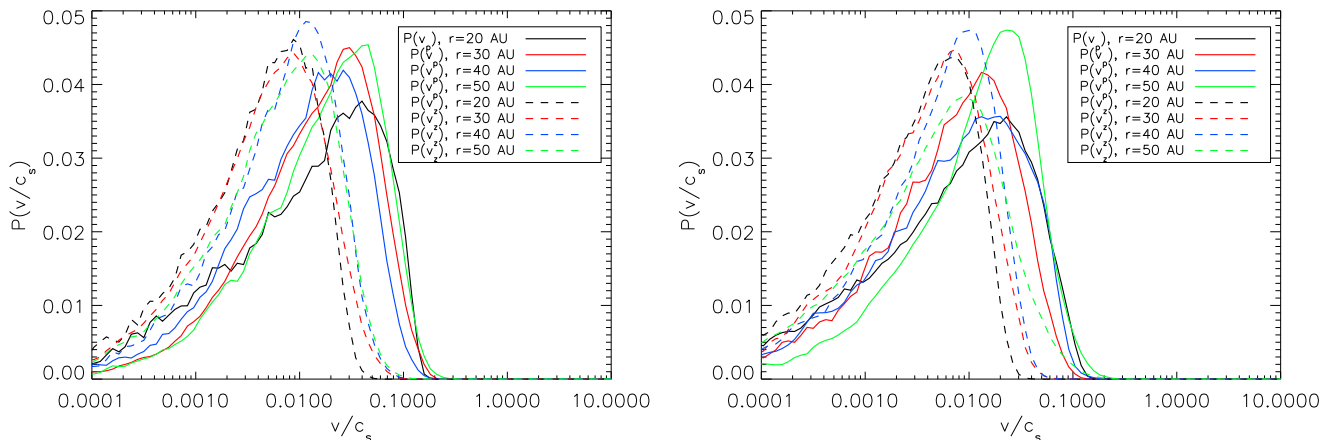


Figure 9. Linewidth probability distributions for Simulation 1 at different numerical resolutions, where rays are drawn at a variety of radii. Planar disc velocities v_p are drawn in solid lines, and vertical velocities v_z are drawn in dashed lines. The left panel indicates the 500,000 particle run, the right panel the one million particle run.

gravitating discs and MRI-driven turbulent discs is the significant separation of v_z and v_p in the self-gravitating case; this robust result is not present in the MRI-driven simulations as v_z and v_p have roughly the same LPD (Simon et al. 2011). As such, it would appear to be a good diagnostic for distinguishing between these two angular momentum transport mechanisms in the limit of low disc mass.

In the high disc mass limit, the LPD fluctuates strongly in v_p as the observation radius is changed because spiral arms move in and out of the annulus. No such fluctuation is detected in v_z , but this is possibly due to resolution effects smoothing them out. The high time variability exhibited by these arms is also apparent in the LPDs as measured across time. This is another feature that was not observed in the simulations of Simon et al. (2011). The angular momentum transport in these simulations was highly local and there were no low m features observed in the LPDs. However, these particular simulations were carried out in the local limit; going to larger scales by performing global MRI simulations may introduce the presence of low m features into the LPD (Beckwith et al. 2011; Simon et al. 2012).

In conclusion, the global simulations carried out in this work suggest that one could potentially distinguish between MRI-driven turbulence and self-gravitational effects by observing the variation of turbulent line width with radius (to potentially probe low m structures) and inclination angle. We must reiterate, however, that our simulations are quite low in resolution, and as such, important phenomenology may not be exhibited. In addition to this, stellar irradiation - an important driver of line emission from the disc surface - is not included as a radiation source. We recommend that local simulations be carried out in much the same manner as Simon et al. (2011). These simulations would be capable of confirming the features of gravito-turbulence seen in the low-mass discs, whose angular momentum transport is locally determined (Forgan et al. 2011). This includes the systematic separation of v_z and v_p . Also, the increase in resolution afforded by local simulations would allow the study of gravito-turbulent broadening as a function of disc altitude, giving a further means of comparison to MRI turbulence. Stellar irradiation must also be considered in future simulations used for linewidth studies. Finally, it is clear that more sophisticated attempts to make synthetic observations of the linewidth broadening are required to determine the detectability of these features using current and future telescopes.

It is also worth noting that while theory indicates that self-gravitating protostellar discs should exist only in the early embedded phase of protostar formation, this does not present an insurmountable obstacle to observing these features. Judicious selection of a line with high critical density for activation should allow the midplane to be probed without contamination from the envelope.

ACKNOWLEDGMENTS

Density plots were produced using SPLASH (Price 2007). Simulations were performed using high performance computing funded by the Scottish Universities Physics Alliance (SUPA). DF gratefully acknowledges support from STFC grant ST/J001422/1. PJA and JBS acknowledge support from NASA (NNX09AB90G, NNX11AE12G) and the NSF (0807471).

REFERENCES

- Altay G., Croft R. A. C., Pelupessy I., 2008, MNRAS, 386, 1931
- Andrews S. M., Williams J. P., 2007, ApJ, 659, 705
- Armitage P. J., 2011, ARA&A, 49, 195
- Armitage P. J., Livio M., Pringle J. E., 2001, MNRAS, 324, 705
- Artymowicz P., Lubow S. H., 1994, ApJ, 421, 651
- Balbus S. A., Hawley J., 1998, Reviews of Modern Physics, 70, 1
- Balbus S. A., Hawley J. F., 1991, ApJ, 376, 214
- Balbus S. A., Papaloizou J., 1999, ApJ, 521, 650
- Bate M. R., Bonnell I. A., Price N. M., 1995, MNRAS, 277, 362
- Beckwith K., Armitage P. J., Simon J. B., 2011, MNRAS, 416, no
- Bell K. R., Lin D. N. C., 1994, ApJ, 427, 987
- Boley A. C., Hartquist T. W., Durisen R. H., Michael S., 2007, ApJ, 656, L89
- Chiang E., Youdin A., 2010, Annual Review of Earth and Planetary Sciences, 38, 493
- Clarke C. J., 2009, MNRAS, 396, 1066
- Cossins P., Lodato G., Clarke C. J., 2009, MNRAS, 393, 1157
- Cossins P., Lodato G., Testi L., 2010, MNRAS, 407, 181
- Durisen R., Boss A. P., Mayer L., Nelson A. F., Quinn T., Rice W. K. M., 2007, in Reipurth B., Jewitt D., Keil K., eds, Protostars and Planets V Gravitational Instabilities in Gaseous Pro-

- toplanetary Disks and Implications for Giant Planet Formation.
University of Arizona Press
- Forgan D., Rice K., Cossins P., Lodato G., 2011, *MNRAS*, 410, 994
- Forgan D. H., Rice K., 2010, *MNRAS*, 406, 2549
- Forgan D. H., Rice K., Stamatellos D., Whitworth A. P., 2009, *MNRAS*, 394, 882
- Gammie C., 2001, *ApJ*, 553, 174
- Gammie C. F., 1996, *ApJ*, 457, 355
- Gingold R. A., Monaghan J. J., 1977, *MNRAS*, 181, 375
- Hartmann L., Calvet N., Gullbring E., D'Alessio P., 1998, *ApJ*, 495, 385
- Hughes M., Wilner D. J., Andrews S. M., Qi C., Hogerheijde M. R., 2011, *ApJ*, 727, 85
- Laughlin G., Bodenheimer P., 1994, *ApJ*, 436, 335
- Lin D. N. C., Pringle J. E., 1987, *MNRAS*, 225, 607
- Lodato G., 2007, *Rivista Del Nuovo Cimento*, 30, 293
- Lodato G., Price D. J., 2010, *MNRAS*, 405, 1212
- Lodato G., Rice W. K. M., 2004, *MNRAS*, 351, 630
- Lodato G., Rice W. K. M., 2005, *MNRAS*, 358, 1489
- Lucy L. B., 1977, *The Astronomical Journal*, 82, 1013
- Martin R. G., Lubow S. H., 2011, *ApJ*, 740, L6
- Mayer L., Lufkin G., Quinn T., Wadsley J., 2007, *ApJ*, 661, L77
- Monaghan J. J., 1992, *ARA&A*, 30, 543
- Monaghan J. J., 2005, *Reports on Progress in Physics*, 68, 1703
- Murray J. R., 1996, *MNRAS*, 279, 402
- Paczynski B., 1978, *Acta Astronomica*, 28, 91
- Papaloizou J. C. B., Nelson R. P., 2003, *MNRAS*, 339, 983
- Price D. J., 2007, *PASA*, 24, 159
- Pringle J. E., 1981, *ARA&A*, 19, 137
- Rafikov R., 2005, *ApJ*, 621, 69
- Rice W. K. M., Armitage P. J., 2009, *MNRAS*, 396, 2228
- Rodríguez L. F., Loinard L., D'Alessio P., Wilner D. J., Ho P. T. P., 2005, *ApJ*, 621, L133
- Shakura N. I., Sunyaev R. A., 1973, *A&A*, 24, 337
- Simon J. B., Armitage P. J., Beckwith K., 2011, *ApJ*, 743, 17
- Simon J. B., Beckwith K., Armitage P. J., 2012, *MNRAS*, 422, 2685
- Stamatellos D., Hubber D. A., Whitworth A. P., 2007, *MNRAS*, 382, L30
- Stamatellos D., Whitworth A. P., 2008, *A&A*, 480, 879
- Stamatellos D., Whitworth A. P., Bisbas T., Goodwin S., 2007, *A&A*, 475, 37
- Toomre A., 1964, *ApJ*, 139, 1217
- Whitehouse S. C., Bate M. R., 2004, *MNRAS*, 353, 1078
- Zhu Z., Hartmann L., Gammie C., McKinney J. C., 2009, *ApJ*, 701, 620